J. Appl. Glycosci., **72**, 7201102 (2025)
doi:10.5458/jag.7201102
©2025 The Japanese Society of Applied Glycoscience

Regular Paper

Kinetics of Structural Changes in Starch Retrogradation Observed by Simultaneous SANS/FTIR–ATR Measurements

(Received August 3, 2024; Accepted November 18, 2024)
(J-STAGE Advance Published Date: February 11, 2025)

Yoshinobu Hirata,[1] Fumitoshi Kaneko,[2] Aurel Radulescu,[3] Takahisa Nishizu,[4,5] Nakako Katsuno,[4] Teppei Imaizumi,[4,5] Ryuhei Motokawa,[6] Takayuki Kumada,[6] and Hiroshi Nakagawa[6,7,†]

[1] *The United Graduate School of Agricultural Science, Gifu University*
(*1−1 Yanagido, Gifu City, Gifu 501−1193, Japan*)
[2] *Graduate School of Science, Osaka University*
(*1−1 Machikaneyama, Toyonaka, Osaka 560−0043, Japan*)
[3] *Forschungszentrum Jülich GmbH, Jülich Centre for Neutron Science* (*JCNS*) *at Heinz Maier-Leibnitz Zentrum* (*MLZ*)
(*Lichtenbergstraße 1, 85747 Garching, Germany*)
[4] *Faculty of Applied Biological Sciences, Gifu University*
(*1−1 Yanagido, Gifu City, Gifu 501−1193, Japan*)
[5] *Preemptive Food Research Center, Gifu University*
(*1−1 Yanagido, Gifu City, Gifu 501−1193, Japan*)
[6] *Materials Sciences Research Center, Japan Atomic Energy Agency*
(*2−4 Shirakata, Tokai, Ibaraki 319−1195, Japan*)
[7] *J-PARC Center, Japan Atomic Energy Agency*
(*2−4 Shirakata, Tokai, Ibaraki 319−1195, Japan*)

Abstract: Because of the complicated hierarchical structure of starch, starch retrogradation is usually evaluated by combining several structural analysis methods covering various spatial scales. However, structural analyses are typically performed individually, making correlating the structural changes at different spatial scales challenging. Therefore, this study used a simultaneous measurement system comprising small-angle neutron scattering (SANS)/Fourier-transform infrared (FTIR)-attenuated total reflection (ATR) to record multiple structural changes in potato starch during retrogradation. In the SANS patterns, the shoulder-like peak became more pronounced with time. The peak intensity, I_{max}, representing the amount of ordered semicrystalline structures, increased over time, revealing the orderly reassembly of starch on the nanoscale upon retrogradation. In the FTIR–ATR spectra, the ratio of absorptions ($R_{1042/1016}$) at 1,042 and 1,016 cm^{-1}, indicating the short-range ordered structure in starch, increased during retrogradation. Therefore, the double-helix structures were reformed during retrogradation. The rate constant of the kinetic change for $R_{1042/1016}$ was larger than for I_{max}; thus, changes in the short-range ordered structure of starch converged before the changes in the semicrystalline structure. These results suggest that the formation of double-helix structures of the amylopectin side chain and the structural change of its ordered arrangement could occur in stages during retrogradation.

Key words: starch, retrogradation, small-angle neutron scattering, FTIR–ATR, simultaneous measurement

INTRODUCTION

Starch retrogradation is the process in which gelatinized starch recrystallizes over time [1−3]. It is an undesirable structural change in food processing because it degrades the texture and shelf life of starchy foods. However, due to the complicated structure of starch, retrogradation is not yet fully elucidated. Starch has a hierarchical structure at various spatial scales [4−6]. Starch granules are semicrystalline and have a layered structure with alternating amorphous and semicrystalline growth rings [7]. Semicrystalline growth rings have a structural periodicity comprising crystalline and amorphous lamellae, and a pair of lamellae is called a cluster [8]. The crystalline regions are described by a short-range ordered structure, with a molecular order related to the double-helix structure [9, 10], and a long-range ordered structure, indicating the overall order of starch crystals in terms of the packing of the double-helix of amylopectin side chains [11, 12].

In starch retrogradation studies, because of the complex hierarchical structure of starch, it is necessary to investigate the structural changes at each scale using appropriate analytical methods. Clarifying the chronological sequence of structural changes revealed in each analysis is essential for

†Corresponding author (Tel. & Fax. +81−29−284−3930, E-mail: nakagawa.hiroshi@jaea.go.jp, ORCID ID 0000-0002-3024-9136).
Abbreviations: SANS, small-angle neutron scattering; FTIR, Fourier-transform infrared; ATR, attenuated total reflection; IR, infrared; SDD, sample-to-detector distance.
This is an open-access paper distributed under the terms of the Creative Commons Attribution Non-Commercial (by-nc) License (CC-BY-NC4.0: https://creativecommons.org/licenses/by-nc/4.0/).

understanding the structural changes in starch retrogradation adequately. However, each experiment is usually performed individually. Although gelatinization can be controlled reproducibly by temperature and moisture content, starch retrogradation is not easily controlled. Starch retrogradation changes over time, and it is difficult to replicate the results exactly, even using the same sample, because the conditions and environment strongly affect the rate and degree of starch retrogradation [13]. Furthermore, it is challenging to correlate the structural information from various methods during retrogradation on a timescale of hours. To overcome this problem, freeze-dried starch samples in which retrogradation has been stopped are used for evaluation, but this method only provides fragmentary information on retrogradation. Therefore, a method for monitoring starch retrogradation in real-time and a native condition through simultaneous measurements would be valuable.

Researchers have used various simultaneous measurement systems in starch studies; for example, small-angle neutron scattering (SANS) is applied because neutrons have high penetration and low energy, avoiding damage to the sample. Doutch et al. measured the loss in lamellar order and starch gel formation using a viscometer and SANS simultaneously [14]. Pullen et al. investigated structural and thermal changes in starch using simultaneous SANS and differential scanning calorimetry measurements [15]. Balacescu et al. developed a simultaneous SANS and Fourier-transform infrared (FTIR) method by transmission [16]. Although they attempted to use this method to observe the starch structure, the infrared (IR) light could not penetrate the starch gel, and the measurement was insufficient. FTIR–attenuated total reflection (ATR) is also frequently used to measure structural changes in starch retrogradation [17−19]. Therefore, FTIR–ATR effectively recorded the structural changes of starch in the present study.

FTIR spectroscopy is suitable for investigating the short-range ordered structure of starch by evaluating the amount of the short-range ordered structures from the absorption ratio of crystalline and amorphous regions [5, 20, 21]. FTIR measures the environment around atoms, and the formation of short-range ordered structures causes changes in the state of functional groups attributed to these two regions. Changes in starch crystallinity on the atomic scale caused by retrogradation that are observed by FTIR are interpreted as changes in the crystalline and amorphous states.

Small-angle scattering (SAS) can be used for examining the clusters of lamellar structures in starch. The SAS pattern of starch shows several diffraction peaks related to the periodic arrangement of clusters in the lamellar structure, and the cluster thickness or lamellar spacing can be observed [8]. The changes in the semicrystalline structure, such as clusters in starch on the nanoscale, owing to retrogradation determined by SAS are interpreted as changes in the double-helix arrangement in that structure.

Because of the hierarchical nature of the starch structure over a wide spatial scale, the structural information obtained by SAS differs from that obtained by FTIR. Although many researchers have reported changes in short-range ordered and semicrystalline structures of starch during retrogradation [22−24], the kinetic relationship between the structures during retrogradation is unclear. Verifying the kinetics by simultaneous SANS and FTIR–ATR measurements may clarify the chronological sequence of structural changes in short-range order and semicrystalline structures caused by retrogradation.

In this study, we performed simultaneous measurements to compare the kinetic information about the semicrystalline structure in starch retrogradation obtained by SANS with that of short-range ordered structures obtained by FTIR–ATR. The order of structural changes at different scales during starch retrogradation was observed. The simultaneous measurement method was effective in determining the correlation between these structural changes associated with retrogradation quantitatively.

MATERIALS AND METHODS

Materials. Rice starch prepared from polished rice, *Hitomebore* (Miyagi, Japan, 2021), using the cold alkaline immersion method [25] was used as the A-type starch. Potato starch (Nacalai Tesque, Inc., Kyoto, Japan) was the B-type starch, and sweet potato starch (Wako Pure Chemical Corporation, Osaka, Japan) was the C-type starch.

Gelatinization of starch. Although D_2O is typically used as a solvent in SANS to avoid the strong incoherent scattering of H_2O, the starch retrogradation rate is faster when starch is gelatinized with D_2O [26]. Thus, in this study, the samples were prepared with H_2O to evaluate the starch retrogradation under natural conditions. Distilled water (3.25 mL) at 25 °C was added to the starch sample (2.5 g) and mixed well. The sample was gelatinized immediately for 60 min at 105 °C in an autoclave (HVE-50LB, HIRAYAMA Manufacturing Corp., Saitama, Japan). The gelatinized sample was cooled at 25 °C for 30 min and was used in the following experiments.

SANS. SANS experiments were performed using the SANS-J instrument at the Japan Research Reactor 3 (JRR-3) at the Japan Atomic Energy Agency (JAEA), Japan [27]. To find the specific structural changes of starch during retrogradation by observing a wider spatial range, SANS was conducted at sample-to-detector distances (SDDs) of 2, 4, and 10 m and neutron wavelengths (λ) of 0.65 nm ($\Delta\lambda/\lambda$ = 15 %). The gelatinized starch samples were placed in 1-mm path-length sample cells with demountable quartz windows and measured after 1 h. The SANS measurements were performed with an SDD at 2 m in the order of potato, rice, and sweet potato starches. Measurements were performed in the same sample order with SDDs of 4 and 10 m without sample exchange and repeated four times over 12 h to evaluate the structural changes in starch. Each raw scattering dataset was corrected for detector sensitivity, electronic background, and empty cell contribution and converted to scattering cross-section data using the software Igor Pro 9 (WaveMetrics Inc., OR, USA).

Simultaneous SANS/FTIR–ATR measurements. Simultaneous SANS/FTIR–ATR measurements were performed using the SANS-J instrument at the JAEA, Japan, as described in the *SANS* section [28]. The SANS measurements were conducted using an SDD of 4 m and neutron λ of 0.65 nm ($\Delta\lambda/\lambda$ = 15 %) to achieve a maximum dynamic Q range of 6×10^{-2}–0.8 nm^{-1}. *In situ* FTIR investigations were conducted during the SANS measurements using an

FTIR spectrometer (VIR 200, JASCO Corporation, Tokyo, Japan) installed at a sample position in an appropriate geometry, enabling simultaneous sample irradiation using IR and neutron coaxial beams (Fig. 1). The IR beam (white arrows in Fig. 1) from the FTIR instrument on the right-hand side, the direction of which was adjusted by a mirror, was incident on the ATR prism in the center at 45°, was reflected five times on the sample surface, and exited to the IR detector on the left-hand side. The sample was irradiated with the neutron beam (black arrows in Fig. 1). The scattered neutron beam passed through the ATR prism to the neutron detector. The ATR sample holder was made of copper and was divided into a lid and a body, and an O-ring between them sealed the sample space. A trapezoidal ZnSe prism (base angle: 45°; length: 30 mm; width: 10 mm; thickness: 3 mm; refractive index: 2.4) for ATR measurements was attached to the lid, and a circular ZnSe window (diameter: 22 mm, thickness: 2 mm) was attached to the body. The sample thickness was adjusted to 1 mm. One hour after cooling, the gelatinized potato starch sample was placed on the ATR crystal surface. The SANS measurement was repeated 12 times continuously, alternating 30 min sample and 3 min transmittance measurements (Fig. 1). The *SANS* section describes the SANS data analysis. The FTIR measurement was repeated 37 times every 15 min continuously, over a scan range of 400–4,000 cm^{-1} at a resolution of 4 cm^{-1}. We determined the peak positions from the second derivative of the spectra by using the spectra manager analysis software provided by JASCO Corporation (third polynomial order and 15 Savitzky–Golay smoothing points).

RESULTS AND DISCUSSION

Changes in the SANS patterns for all starches. Starches are classified as A-type, B-type, and C-type based on X-ray diffraction (XRD) patterns, and each has a different retrogradation rate [25]. This study measured rice starch as an A-type starch, potato starch as a B-type starch, and sweet potato starch as a C-type starch for SANS to select starch samples that change hourly. Figure 2 shows the SANS patterns (I, Q) of the starch samples, where I and Q are the scattering intensity and amplitude of the scattering vector, respectively. No change in the rice starch scattering pattern with time was observed in all Q ranges during the measurement. However, the potato and sweet potato starch scattering intensities increased with time in Q ranges from 0.08 to 0.6 nm^{-1} and 0.03 to 0.5 nm^{-1}, respectively. The retrogradation rate is the fastest for B-type starch and the slowest for A-type starch [25]. The sweet potato starch scattering intensity increased in the low-Q region compared with that of potato starch, and the changes in the SANS patterns differed. The intensity gradually decreased from the low- to high-Q region, reflecting changes in the aggregated structures in the starch samples [29]. SANS intensity is correlated with the density of nuclei, and a stronger SANS intensity reflects higher ordering of aggregated structures. Thus, the increase in intensity in the low-Q region indicated that the aggregates formed by retrogradation grew in sweet potato starch. A shoulder-like peak appeared at Q = 0.2–0.3 nm^{-1} in potato starch, consistent with small-angle X-ray scattering (SAXS) of starch recrystallization owing to retrogradation [23, 30]. Although the restored structure differed from the native structure, this result showed that semicrystalline-like structures formed. Simultaneous measurements using potato starch were

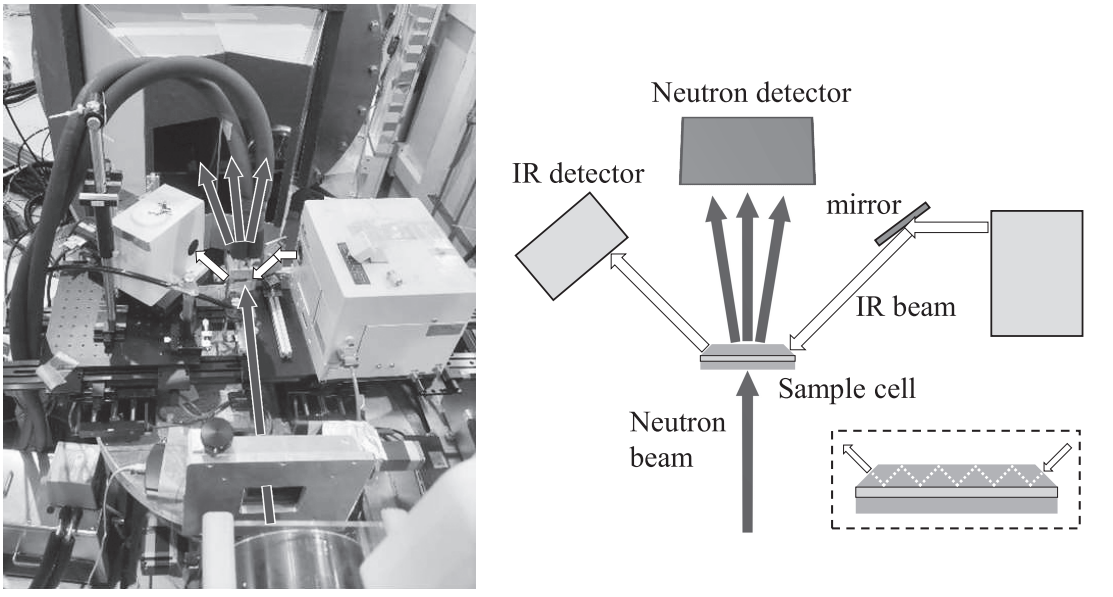

Fig. 1. Photograph (left), schematic (right), and schedule (bottom) of the simultaneous SANS/FTIR–ATR measurement system.
The white and black arrows indicate the IR and neutron beams, respectively.

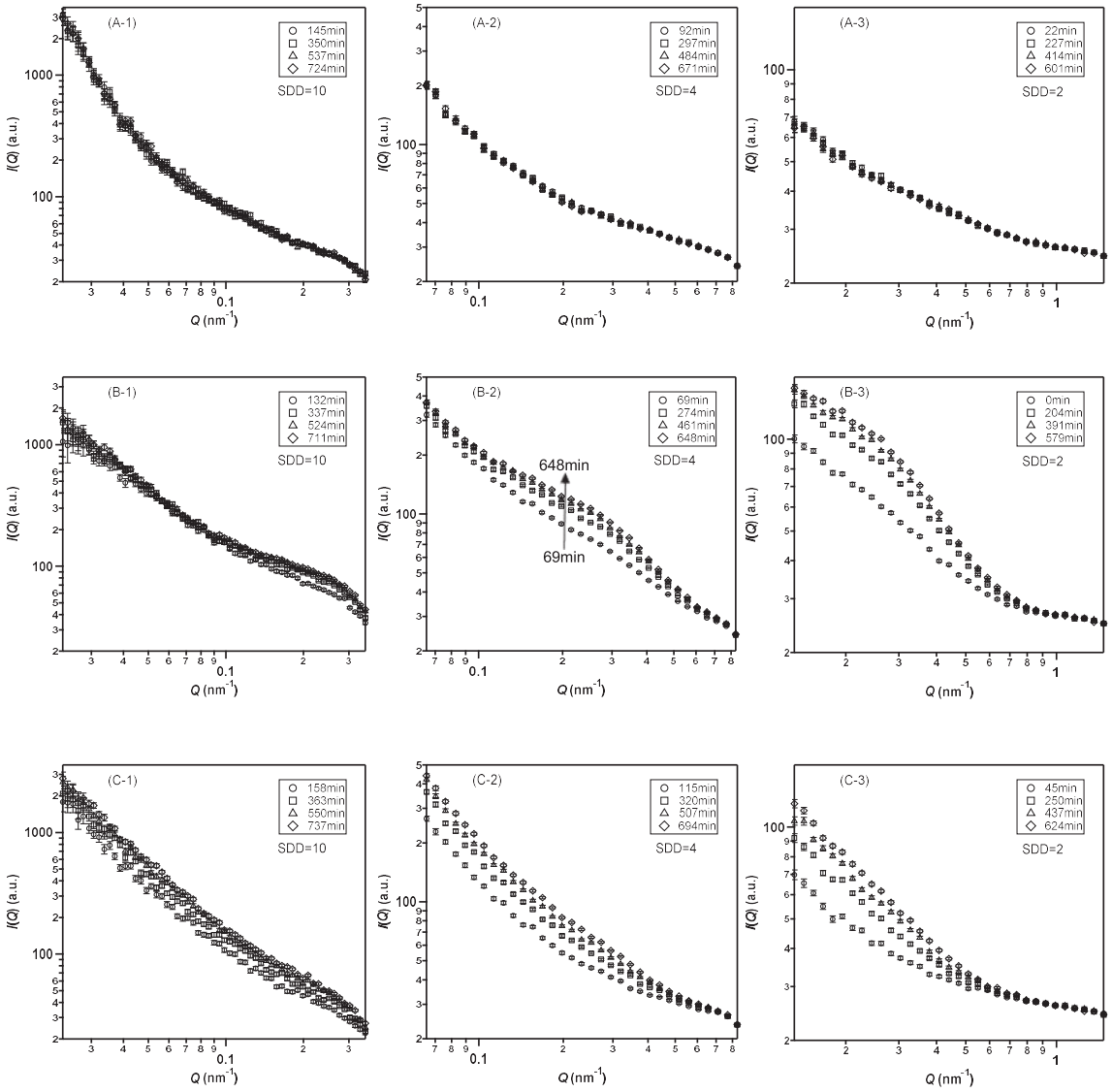

Fig. 2. SANS patterns of (A) rice, (B) potato, and (C) sweet potato starches. SDD is indicated in m; the legend represents the time passed.

conducted to investigate the relationship between lamellae and short-range order during retrogradation. Simultaneous SANS/FTIR–ATR measurements were performed using an SDD of 4 m for potato starch to focus on the shoulder peak of starch because the change could be observed in the Q region.

Changes in SANS patterns during simultaneous measurements. Figure 3A shows potato starch SANS patterns (I, Q) for the simultaneous SANS and FTIR–ATR measurements. As described in the *Changes in the SANS patterns for all starches* section, the scattering intensity gradually increased, and a shoulder-like peak appeared at Q = 0.2–0.3 nm^{-1}. The shoulder-like peak became more pronounced with time, indicating that a semicrystalline-like structure appeared during retrogradation, as in Fig. 2B-2.

Figure 3B shows the transmittance transition over time. The transmittance values, which remained unchanged at approximately 36 %, confirmed the hermeticity of the sample cell. The very low transmittance values may have resulted from the incoherent scattering of H_2O. As mentioned in the *Gelatinization of starch* section, the samples were prepared with H_2O to evaluate the starch retrogradation under natural conditions. The incoherent scattering of H_2O has a constant intensity irrespective of Q, meaning that the Q dependence of the SANS profile was attributed to coherent scattering from the starch structure and could be used for structural analysis.

The shoulder-like peak based on the semicrystalline model was quantitatively analyzed by model fitting of the SANS profile based on the Cauchy and power law functions (Eq. 1) [8, 24],

$$I(Q) = I_{max}\left[1+4\left(\frac{Q-Q_1}{\Delta Q}\right)^2\right]^{-1} + AQ^{-\alpha} + B \quad (1)$$

where I_{max} is the peak intensity, Q_1 is the maximum peak position, ΔQ is the full width at half maximum of the peak, α is the fractal coefficient, and A and B are positive adjustable parameters.

Many SAXS studies have focused on I_{max}, which is related to the amount of semicrystalline structures, Q_1, reflecting the lamellae spacing, and α, representing the fractal dimension [24, 31, 32]. When the data were initially fitted without the parameter fixed, ΔQ, A, and B were near constant over time. This study improved the accuracy of the I_{max}, Q_1, and α values by fitting the SANS patterns with ΔQ, A, and B set as the averaged values of all fitting data

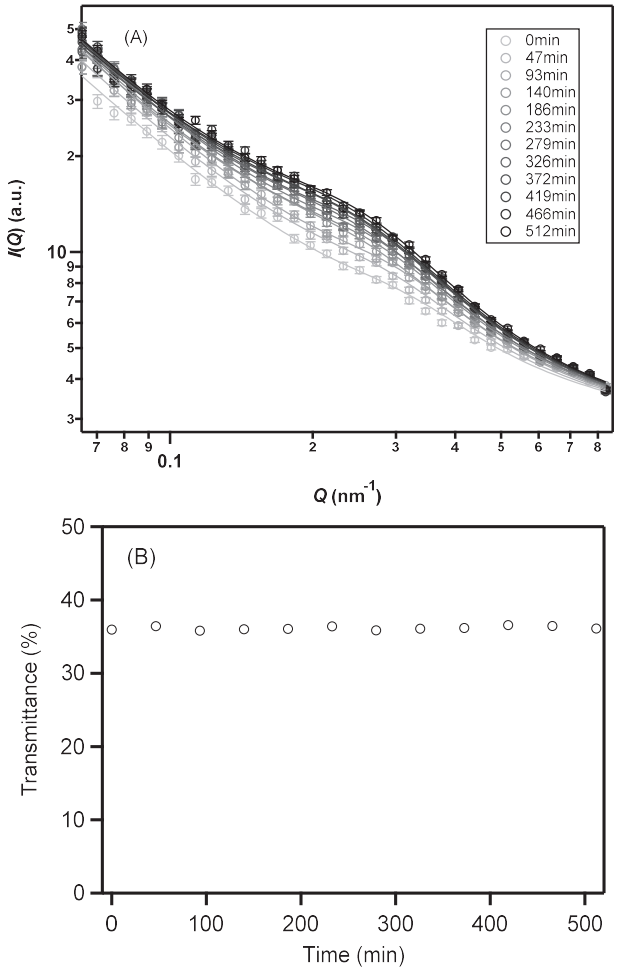

Fig. 3. (A) SANS patterns of potato starch and the fitting curves obtained using Eq. (1). (B) Transmittance values determined by SANS.

(ΔQ = 0.317802 nm^{-1}, A = 0.62911, and B = 2.722267) (Fig. 3A). Furthermore, Q_1 was obtained by fitting the SANS patterns with I_{max} and α set to improve accuracy. Figure 4 shows the changes in the I_{max}, Q_1, and α values obtained by Eq. (1) over time. The I_{max} value was initially 1.42 but increased over time and reached 6.01. I_{max} depends on the amount of ordered semicrystalline structures and enables qualitative comparison of the degree of order of starch molecules [8, 32]. This result showed that the amount of regularly arranged double helical structures increased over time, and thus that the starch was regularly reassembled at the nanoscale during retrogradation. The Q_1 value decreased slightly from 0.273 at the beginning to approximately 0.206 at the end, indicating that the peak position shifted from the high- to low-Q regions. This result indicates that the spacing between lamellae gradually increased slightly during retrogradation. In previous studies, the α value was used to evaluate the compactness of the starch structure [23, 24]. The α value increased slightly from 1.44 to approximately 1.52, which was attributed to the increased compactness of the starch structure caused by retrogradation. These results are consistent with the trends observed in previous SAXS studies [24].

FTIR–ATR spectral changes during simultaneous measurements. Figure 5A shows the FTIR spectral changes of potato starch during retrogradation. The FTIR spectrum shape was similar to that of the starch hydration samples in a previous study [19]. Absorbance at 1,047 and 1,022 cm^{-1} reflects the crystalline and amorphous regions of starch, respectively [9]. These bands indicate the bending of the –COH and –CH_2 groups in starch. The intensity ratio of the 1,047 to the 1,022 cm^{-1} peak, $R_{1047/1022}$, is frequently used to evaluate the crystallinity and the short-range order in starch

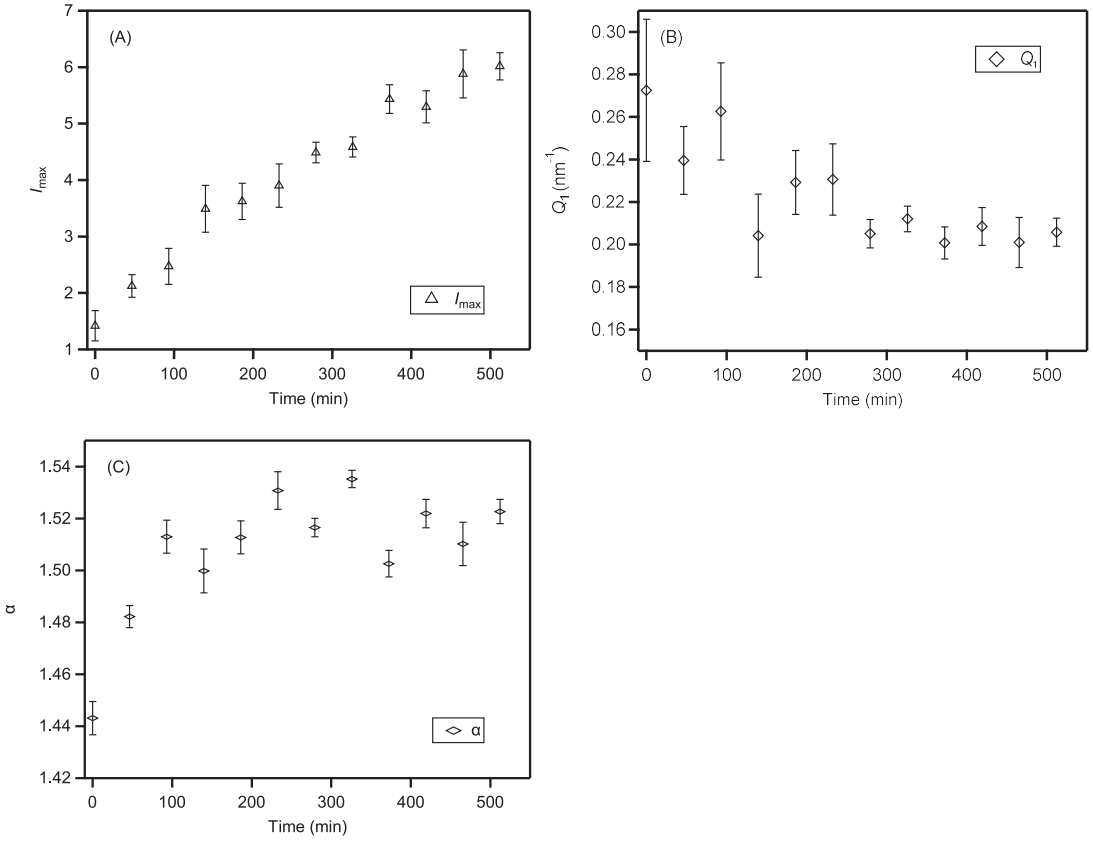

Fig. 4. Values of (A) I_{max} (△), (B) Q_1 (◇), and (C) α (<>) determined by Eq. (1).

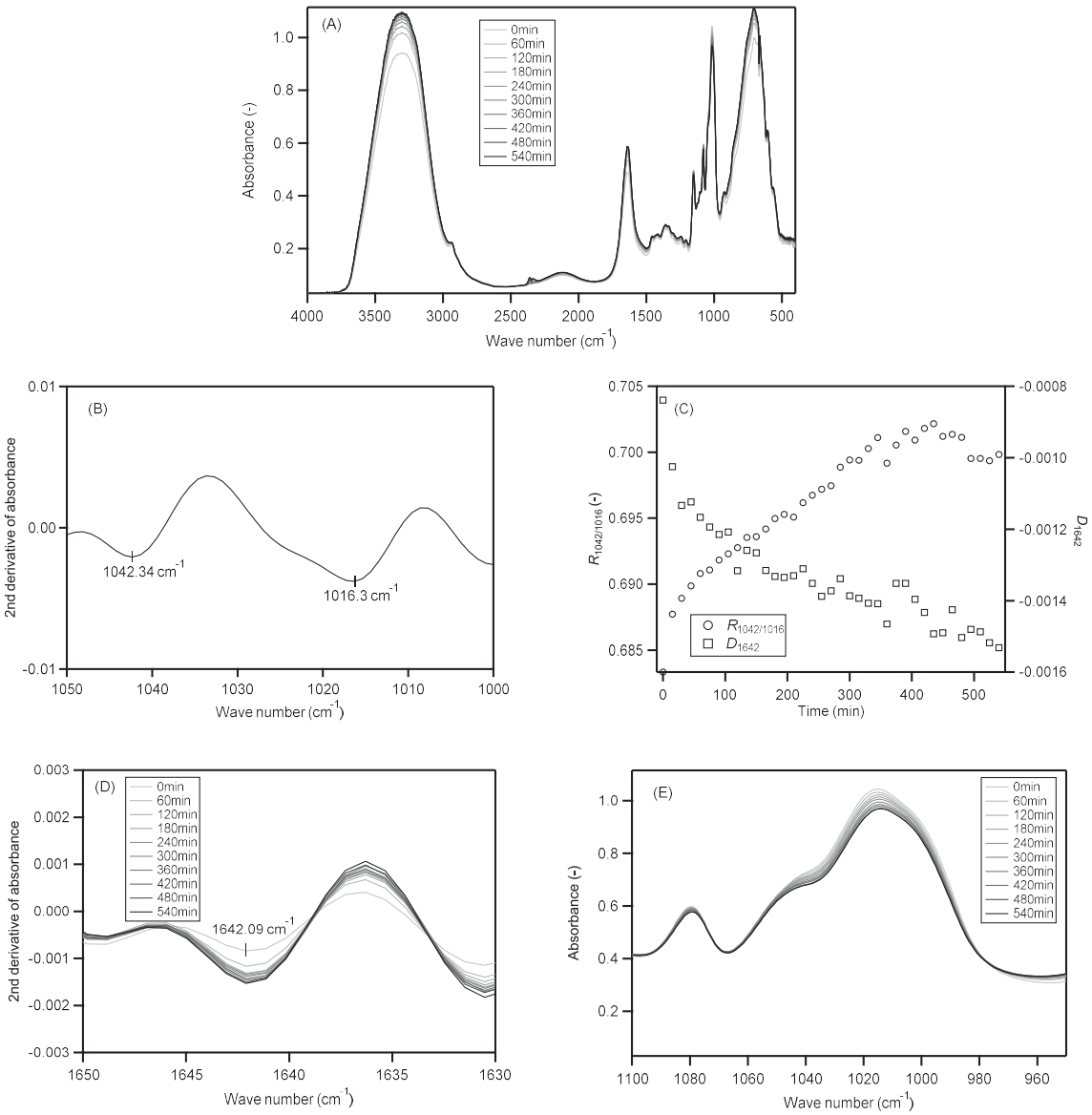

Fig. 5. (A) FTIR–ATR spectra of potato starch for all ranges. (B) Second-derivative spectra from 1,000 to 1,050 cm^{-1} obtained by Spectra Manager analysis software (JASCO Corporation). (C) $R_{1042/1016}$ value (○) and D_{1642} value (□) determined by FTIR–ATR. (D) Second-derivative spectra from 1,630 to 1,650 cm^{-1} obtained by Spectra Manager analysis software. (E) FTIR–ATR spectra of potato starch from 950 to 1,100 cm^{-1}.

samples [5, 20, 21]. In the present study, the peak positions were determined at 1,042 and 1,016 cm^{-1} by the second derivative (Fig. 5B). The $R_{1042/1016}$ value increased over time (Fig. 5C), confirming that the short-range ordered structure in starch increased during retrogradation, consistent with previous studies [22, 33−35]. Bai et al. reported that the decrease in the $R_{1047/1022}$ value indicated a decrease in the formation of double-helix structures [35]. Thus, the changes in $R_{1042/1016}$ indicated the formation of double-helix structures in starch during retrogradation, which led to a change in the frequency of the bending of the –COH and $–CH_2$ groups in starch.

The broad absorption from 3,000 to 3,700 cm^{-1} derives from the O–H stretching modes of starch and water [22, 36−38]. As in a previous study, the water absorption band for hydrated starch overlapped with the peaks related to starch from 3,000 to 3,700 cm^{-1} [19]. Although the absorbance increased over time in this frequency range (Fig. 5A), it was difficult to distinguish whether this spectral change arose from starch and water or water alone. However, the absorption peak around 1,640 cm^{-1} from the OH-bending vibration of water molecules is related to the water content of the sample and does not overlap with the absorbance of starch [36, 39]. This absorbance also increased over time (Fig. 5A). The peak position was determined as 1,642 cm^{-1} by the second derivative (Fig. 5D). The second derivatives of the absorbance at 1,642 cm^{-1} (D_{1642}) were calculated to eliminate the effect of the baseline, and the D_{1642} value decreased over time (Fig. 5C). Because the ATR method observes the surface of the prism, the decrease in D_{1642} suggested an increase in the observed water absorbance on the surface of the prism. In addition, the constant SANS transmittance confirmed the hermeticity of the sample cell (Fig. 3B); therefore, there was no effect from water evaporation during the measurement, and the change in D_{1642} indicated that the water in the starch was leaving the sample and collecting on the surface of ATR prism. Potato starch recrystallizes over a timescale of hours [25]. The recovery of the crystalline structure means that the hydrogen bonds between the starch and water are broken, implying the release of water.

Consequently, water release could have occurred within the measurement time in this study, and the change in D_{1642} indicated water release owing to recrystallization. Retrogradation expels water from the gelatinized starch [40]. Zhang et al. reported that in low-field NMR imaging, the water in starch gel migrated outward from the center of the gel with storage time [41]. These previous observations are consistent with our results. Figure 5E shows that the absorbances at 1,042 and 1,016 cm^{-1} were reduced, which could be caused by the aggregation of starch and the release of water by retrogradation, reducing the starch density on the sample surface. However, this phenomenon contributed less to these ratios and did not affect the quantification of short-range ordered structures as determined by FTIR–ATR. The FTIR–ATR results showed an increase in the short-range ordered structures and water release of the sample by retrogradation. Simultaneous SANS/FTIR–ATR measurements with a tightly sealed sample cell allowed us to track the structural changes in starch and changes in water release over time simultaneously.

Relationship between structural changes at different spatial scales and dehydration. The rate constants of structural changes for each parameter can be determined using I_{max} from SANS and $R_{1042/1016}$ and D_{1642} from FTIR–ATR. We expected that analyzing the rate constants would provide information on the order in which each structural change occurs in starch retrogradation. Figure 6 plots I_{max} determined by SANS and $R_{1042/1016}$ and D_{1642} determined by FTIR–ATR. Many researchers have used the Avrami equation to evaluate the kinetic changes in the ordered and crystalline structures of retrograded starch [42, 43]. The retrogradation degree of potato starch converges to equilibrium [25]. Therefore, we compared these rate constants easily by fitting the data using a modified version of the Avrami equation (Eq. 2), where the exponent was equal to 1, as in previous studies [44, 45], and the time to obtain half the equilibrium value was calculated as

$$\frac{a-y}{a-y_i}=\exp(-kt) \tag{2}$$

where a is the equilibrium value, y is I_{max} for SANS and $R_{1042/1016}$ and D_{1642} for FTIR–ATR, y_i is the initial of y, k is the rate constant, and t is the storage time.

The k values were 0.0018 ± 0.0006 min^{-1} for I_{max}, 0.0050 ± 0.0006 min^{-1} for $R_{1042/1016}$, and 0.0064 ± 0.0010 min^{-1} for D_{1642}. The time to obtain half the equilibrium value was 383.3 min for I_{max}, 138.0 min for $R_{1042/1016}$, and 108.3 min for D_{1642}. The double-helix formation, regular helix alignment, and water release proceeded simultaneously after gelatinization but at different rates. The time required to obtain half the equilibrium value for $R_{1042/1016}$ was less than for I_{max}, indicating that the changes in the short-range ordered structure in starch observed by FTIR–ATR converged before changes in the nanostructure observed by SANS. These results show that the formation of the double-helix structures in the amylopectin side chain and the structural change in its ordered arrangement could occur in stages. In other words, there was a transient state during retrogradation where double helixes were formed but with disordered arrangements. The time required to reach half the equilibrium of D_{1642} was faster than that of I_{max} and $R_{1042/1016}$. Water release from the gelatinized starch was completed before the structural changes in the starch during retrogradation.

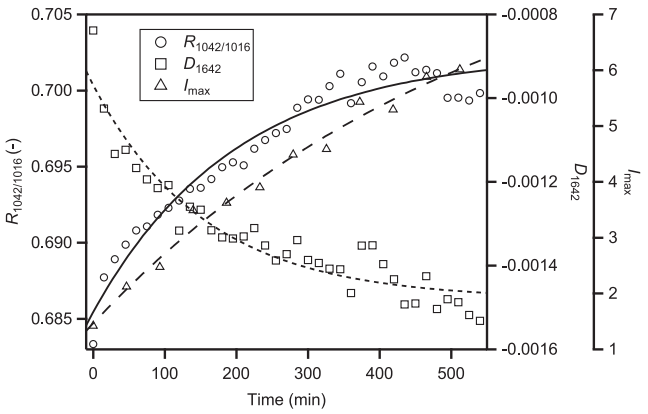

Fig. 6. I_{max} value measured by SANS (–△–) fitted with Eq. (2), and the $R_{1042/1016}$ (–⊖–) and D_{1642} values (-·-□-·) measured by FTIR-ATR for both sequences.

CONCLUSIONS

This study evaluated multiple structural changes during potato starch retrogradation using a simultaneous SANS/FTIR–ATR measurement system. The SANS shoulder-like peak became more pronounced over time, indicating that retrogradation formed semicrystalline-like structures. The SANS analysis results based on the Cauchy and power law functions showed that I_{max} increased over time, revealing the orderly reassembly of starch on the nanoscale upon retrogradation, increasing the amount of ordered double helical structures. In the FTIR–ATR spectra, $R_{1042/1016}$ increased and D_{1642} decreased over time, confirming an increase in the short-range ordered structures in starch and water release from the sample during retrogradation. Comparing the time required to obtain half the equilibrium value showed that water release was completed before the structural changes in the starch during retrogradation. Furthermore, changes in the short-range ordered structures of starch observed by FTIR–ATR converged before changes in the semicrystalline structure observed by SANS. These simultaneous SANS/FTIR–ATR measurements showed that the formation of the double-helix structures of the amylopectin side chain and the structural change in its ordered arrangement could occur in stages during retrogradation. The simultaneous measurement method allowed quantitative discussion of the correlation between these different structural changes associated with retrogradation, which is a major technical achievement.

ACKNOWLEDGMENTS

The neutron experiment at the JRR-3 was performed using a user program (proposal nos. 2022A-A41, D458, D463, and D615). This work was partly supported by the JSPS KAKENHI Grant Numbers 24KJ1210, JP20H02944 and 20KK0350. We thank Amy Capes, PhD, from Edanz (https://jp.edanz.com/ac) for editing a draft of this manuscript.

CONFLICTS OF INTEREST

The authors declare no conflict of interests.

REFERENCES

[1] Chang Q, Zheng B, Zhang Y, Zeng H. A comprehensive review of the factors influencing the formation of retrograded starch. Int J Biol Macromol. 2021; 186: 163−73.

[2] Donmez D, Pinho L, Patel B, Desam P, Campanella OH. Characterization of starch–water interactions and their effects on two key functional properties: starch gelatinization and retrogradation. Curr Opin Food Sci. 2021; 39: 103−9.

[3] Karim AA, Norziah MH, Seow CC. Methods for the study of starch retrogradation. Food Chem. 2000; 71: 9−36.

[4] Bertoft E. Understanding starch structure: Recent progress. Agronomy. 2017; 7: 56.

[5] Chi C, Li X, Huang S, Chen L, Zhang Y, Li L, et al. Basic principles in starch multi-scale structuration to mitigate digestibility: A review. Trends Food Sci Technol. 2021; 109: 154−68.

[6] Junejo SA, Flanagan BM, Zhang B, Dhital S. Starch structure and nutritional functionality – Past revelations and future prospects. Carbohydr Polym. 2022; 277: 118837.

[7] Blazek J, Gilbert EP. Application of small-angle X-ray and neutron scattering techniques to the characterisation of starch structure: A review. Carbohydr Polym. 2011; 85: 281−93.

[8] Yuryev VP, Krivandin AV, Kiseleva VI, Wasserman LA, Genkina NK, Fornal J, et al. Structural parameters of amylopectin clusters and semi-crystalline growth rings in wheat starches with different amylose content. Carbohydr Res. 2004; 339: 2683−91.

[9] van Soest JJ, Tournois H, de Wit D, Vliegenthart JF. Short-range structure in (partially) crystalline potato starch determined with attenuated total reflectance Fourier-transform IR spectroscopy. Carbohydr Res. 1995; 279: 201−14.

[10] Mutungi C, Onyango C, Doert T, Paasch S, Thiele S, Machill S, et al. Long- and short-range structural changes of recrystallised cassava starch subjected to *in vitro* digestion. Food Hydrocoll. 2011; 25: 477−85.

[11] Lu H, Tian Y, Ma R. Assessment of order of helical structures of retrograded starch by Raman spectroscopy. Food Hydrocoll. 2023; 134: 108064.

[12] Pozo C, Rodríguez-Llamazares S, Bouza R, Barral L, Castaño J, Müller N, et al. Study of the structural order of native starch granules using combined FTIR and XRD analysis. J Polym Res. 2018; 25: 266.

[13] Wang S, Li C, Copeland L, Niu Q, Wang S. Starch retrogradation: a comprehensive review. Compr Rev Food Sci Food Saf. 2015; 14: 568−85.

[14] Doutch J, Bason M, Franceschini F, James K, Clowes D, Gilbert EP. Structural changes during starch pasting using simultaneous Rapid Visco Analysis and small-angle neutron scattering. Carbohydr Polym. 2012; 88: 1061−71.

[15] Pullen SA, Booth N, Olsen SR, Day B, Franceschini F, Mannicke D, et al. Design and implementation of a differential scanning calorimeter for the simultaneous measurement of small angle neutron scattering. Meas Sci Technol. 2014; 25: 055606.

[16] Balacescu L, Brandl G, Kaneko F, Schrader TE, Radulescu A. Light scattering and absorption complementarities to neutron scattering: In situ FTIR and DLS techniques at the high-intensity and extended Q-range SANS diffractometer KWS-2. Appl Sci. 2021; 11: 5135.

[17] Yang S, Dhital S, Shan CS, Zhang MN, Chen ZG. Ordered structural changes of retrograded starch gel over long-term storage in wet starch noodles. Carbohydr Polym. 2021; 270: 118367.

[18] Wang S, Li C, Zhang X, Copeland L, Wang S. Retrogradation enthalpy does not always reflect the retrogradation behavior of gelatinized starch. Sci Rep. 2016; 6: 20965.

[19] Warren FJ, Gidley MJ, Flanagan BM. Infrared spectroscopy as a tool to characterise starch ordered structure—a joint FTIR–ATR, NMR, XRD and DSC study. Carbohydr Polym. 2016; 139: 35−42.

[20] Wang H, Ding J, Xiao N, Liu X, Zhang Y, Zhang H. Insights into the hierarchical structure and digestibility of starch in heat-moisture treated adlay seeds. Food Chem. 2020; 318: 126489.

[21] Li Y, He Z, Tu Y, Chen L, Li X. Understanding synchronous regulating effects of starch-protein interactions on starch digestion and retrogradation under thermal shear processing. Carbohydr Polym. 2024; 329: 121767.

[22] Lu H, Ma R, Chang R, Tian Y. Evaluation of starch retrogradation by infrared spectroscopy. Food Hydrocoll. 2021; 120: 106975.

[23] Ma Z, Ma M, Zhou D, Li X, Hu X. The retrogradation characteristics of pullulanase debranched field pea starch: Effects of storage time and temperature. Int J Biol Macromol. 2019; 134: 984−92.

[24] Zhang L, Li X, Janaswamy S, Chen L, Chi C. Further insights into the evolution of starch assembly during retrogradation using SAXS. Int J Biol Macromol. 2020; 154: 521−7.

[25] Taguchi T, Onishi M, Katsuno N, Miwa N, Oomoto C, Sato M, et al. Evaluation of starch retrogradation by X-ray diffraction using a water-addition method. LWT. 2023; 173: 114341.

[26] Hirata Y, Nakagawa H, Yamauchi H, Kaneko K, Hagihala M, Yamaguchi H, et al. Effect of starch retrogradation on molecular dynamics of cooked rice by quasi-elastic neutron scattering. Food Hydrocoll. 2023; 141: 108728.

[27] Kumada T, Motokawa R, Oba Y, Nakagawa H, Sekine Y, Micheau C, et al. Upgrade of the small-angle neutron scattering diffractometer SANS-J at JRR-3. J Appl Crystallogr. 2023; 56: 1776−83.

[28] Kaneko F, Radulescu A, Nakagawa H. Simultaneous SANS/FTIR measurement system incorporating the ATR sampling method. J Appl Crystallogr. 2023; 56: 1522−7.

[29] Lu P, Li X, Janaswamy S, Chi C, Chen L, Wu Y, et al. Insights on the structure and digestibility of sweet potato starch: Effect of postharvest storage of sweet potato roots. Int J Biol Macromol. 2020; 145: 694−700.

[30] Dang Y, Imaizumi T, Nishizu T, Anandalakshmi R, Katsuno N. Effect of the addition of pregelatinized rice starch paste on the retrogradation of rice starch gel. Food Hydrocoll. 2023; 145: 109159.

[31] Yu M, Zhu S, Zhong F, Zhang S, Du C, Li Y. Insight into the multi-scale structure changes and mechanism of corn starch modulated by different structural phenolic acids

during retrogradation. Food Hydrocoll. 2022; 128: 107581.
[32] Liu W, Zhao R, Liu Q, Zhang L, Li Q, Hu X, et al. Relationship among gelatinization, retrogradation behavior, and impedance characteristics of potato starch. Int J Biol Macromol. 2023; 227: 354−64.
[33] An H, Ma Q, Zhang F, Zhai C, Sun J, Tang Y, et al. Insight into microstructure evolution during starch retrogradation by infrared and Raman spectroscopy combined with two-dimensional correlation spectroscopy analysis. Food Hydrocoll. 2024; 146: 109174.
[34] Huang S, Chao C, Yu J, Copeland L, Wang S. New insight into starch retrogradation: The effect of short-range molecular order in gelatinized starch. Food Hydrocoll. 2021; 120: 106921.
[35] Bai J, Zhang L, Jia X, Ye Q, Pei J, Song Q, et al. Multiscale structural changes and mechanistic analysis of wheat starch gels with common proteins in short-term retrogradation at low temperature. Food Hydrocoll. 2024; 146: 109160.
[36] Zhang X, Chen Y, Huang R, Zhang J, Xiong C, Huang G. Study on the effect of different concentrations of choline glycine ionic liquid-water mixtures on debranched starch butyrylation reaction. Carbohydr Polym. 2023; 308: 120680.
[37] Ye Q, Meng X, Pang L. D_2O assisted FTIR spectroscopic analysis of moisture in edible oil. Food Chem X. 2023; 18: 100679.
[38] Nie H, Li C, Liu PH, Lei CY, Li JB. Retrogradation, gel texture properties, intrinsic viscosity and degradation mechanism of potato starch paste under ultrasonic irradiation. Food Hydrocoll. 2019; 95: 590−600.
[39] Xiong J, Li Q, Shi Z, Ye J. Interactions between wheat starch and cellulose derivatives in short-term retrogradation: Rheology and FTIR study. Food Res Int. 2017; 100: 858−63.
[40] Chakraborty I, Govindaraju I, Kunnel S, Managuli V, Mazumder N. Effect of storage time and temperature on digestibility, thermal, and rheological properties of retrograded rice. Gels. 2023; 9: 142.
[41] Zhang Y, Yang T, Zhou J, Yu J, Wang J, Qiang S, et al. Effect of water content on rice starch gel during retrogradation. Starch/Stärke. 2024; 76: 2200268.
[42] Hu Y, He C, Zhang M, Zhang L, Xiong H, Zhao Q. Inhibition from whey protein hydrolysate on the retrogradation of gelatinized rice starch. Food Hydrocoll. 2020; 108: 105840.
[43] Zhang H, Sun B, Zhang S, Zhu Y, Tian Y. Inhibition of wheat starch retrogradation by tea derivatives. Carbohydr Polym. 2015; 134: 413−7.
[44] Berski W, Ziobro R, Witczak M, Gambuś H. The retrogradation kinetics of starches of different botanical origin in the presence of glucose syrup. Int J Biol Macromol. 2018; 114: 1288−94.
[45] Dang LTK, Imaizumi T, Nishizu T. Effects of transglutaminase on the retrogradation of wheat flour. Food Hydrocoll. 2024; 152: 109924.